Heliyon 10 (2024) e30406

Contents lists available at ScienceDirect

Heliyon

journal homepage: www.cell.com/heliyon

Research article

Cortical signals analysis to recognize intralimb mobility using modified RNN and various EEG quantities

Maged S. AL-Quraishi [a], Wooi Haw Tan [b,*], Irraivan Elamvazuthi [c], Chee Pun Ooi [b], Naufal M. Saad [c], Mohammed Isam Al-Hiyali [c], H.A. Karim [b], Syed Saad Azhar Ali [a,d]

[a] *Interdisciplinary Research Center for Smart Mobility and Logistics (IRC-SML), King Fahd University of Petroleum & Minerals (KFUPM), Dhahran, 31261, Saudi Arabia*
[b] *Center of Digital Home, Faculty of Engineering, Multimedia University, 63100, Cyberjaya, Selangor, Malaysia*
[c] *Department of Electrical and Electronic Engineering, Universiti Teknologi PETRONAS, Bandar Seri Iskandar, 36210, Perak, Malaysia*
[d] *Aerospace Engineering Department, King Fahd University of Petroleum & Minerals (KFUPM), Dhahran, 31261, Saudi Arabia*

A R T I C L E I N F O

Keywords:
EEG
Intralimb movement
Deep leaning
Machine learning
Rehabilitation

A B S T R A C T

Electroencephalogram (EEG) signals are critical in interpreting sensorimotor activities for predicting body movements. However, their efficacy in identifying intralimb movements, such as the dorsiflexion and plantar flexion of the foot, remains suboptimal. This study aims to explore whether various EEG signal quantities can effectively recognize intralimb movements to facilitate the development of Brain-Computer Interface (BCI) devices for foot rehabilitation. This research involved twenty-two healthy, right-handed participants. EEG data were collected using 21 electrodes positioned over the motor cortex, while two electromyography (EMG) electrodes recorded the onset of ankle joint movements. The study focused on analyzing slow cortical potential (SCP) and sensorimotor rhythms (SMR) in alpha and beta bands from the EEG. Five key features—fourth-order Autoregressive feature, variance, waveform length, standard deviation, and permutation entropy—were extracted. A modified Recurrent Neural Network (RNN) including Long Short-term Memory (LSTM) and Gated Recurrent Unit (GRU) algorithms was developed for movement recognition. These were compared against conventional machine learning algorithms, including nonlinear Support Vector Machine (SVM) and k Nearest Neighbourhood (kNN) classifiers. The performance of the proposed models was assessed using two data schemes: within-subject and across-subjects. The findings demonstrated that the GRU and LSTM models significantly outperformed traditional machine learning algorithms in recognizing different EEG signal quantities for intralimb movement. The study indicates that deep learning models, particularly GRU and LSTM, hold superior potential over standard machine learning techniques in identifying intralimb movements using EEG signals. Where the accuracies of LSTM for within and across subjects were 98.87 ± 1.80 % and 87.38 ± 0.86 % respectively. Whereas the accuracy of GRU within and across subjects were 99.18 ± 1.28 % and 86.44 ± 0.69 % respectively. This advancement could significantly benefit the development of BCI devices aimed at foot rehabilitation, suggesting a new avenue for enhancing physical therapy outcomes.

* Corresponding author.
E-mail address: twhaw@mmu.edu.my (W.H. Tan).

https://doi.org/10.1016/j.heliyon.2024.e30406
Received 3 January 2024; Received in revised form 17 April 2024; Accepted 25 April 2024
Available online 30 April 2024

1. Introduction

The brain-machine interface (BMI) is a tool that facilitates communication between humans and machines. It is intended to assist disabled individuals with limited motor control due to illness or injury but normal mental function [1–3], Invasive methods, such as inserting microelectrodes into the brain, can be used to interpret neuronal signals from the brain to peripheral devices. However, non-invasive approaches are considered to reduce the medical risks associated with microelectrode insertion. Functional magnetic resonance imaging (fMRI) [4,5], magnetoencephalography (MEG) [6,7],electroencephalography (EEG) [8,9],and functional near-infrared spectroscopy (fNIRS) [10] are the primary non-invasive modalities used in brain imaging techniques [11,12]. Each form of brain imaging has its own distinct benefits and drawbacks. Cost, weight, portability, and the required temporal and spatial resolution for a particular activity or application play a role in selecting a BMI system. EEG is one of the most common electrophysiological signals used in neural rehabilitation and Human-Robot Interaction (HRI) [13]. EEG can be used by both healthy and disabled people to send commands directly from the brain, bypassing physical neural connections such as peripheral nerves and muscles that are not working properly. Numerous methods for assessing motion intention using EEG in a BMI have been studied (both actual and imagined). To achieve closed-loop control, the user's motion intentions (real, attempted, or imagined) must be detected from the brain signals with an extremely short latency. The EEG slow cortical potential (SCP) is a representation of cerebral activity during movement planning and preparation [14,15]. Numerous studies have been conducted to examine SCP using cue-based or self-paced paradigms [16]. On the one hand, studies have shown that SCPs can be used to identify movement in the legs. Niazi et al. [17] used offline recordings to find the SCP during motor execution (ME) and motor imagery (MI) in healthy people, as well as during motor attempts in patients. Additionally, the viability of eliminating extensive training in asynchronous BMIs based on SCP was investigated. The ability to decode lower extremity limb motions using EEG has recently been demonstrated by researchers, highlighting the potential for creating an EEG-based BMI to regain mobility following paralysis. A. Kline et al. [18] used EEG signals from sensorimotor areas (C1 and C2) and parietal cortex areas (PO3 and PO4) to differentiate between left and right leg movements. Tomoyuki et al. [19] employed a classification technique to categorize the brain processes. As decoder inputs, they employed covariance matrices of the computed EEG signals. The EEG signals of the subjects were used to identify their walking intentions and to regulate the movements of the exoskeleton. The gait motion state was decoded using a classification paradigm applying sparse discriminant analysis (SDA), which performs linear discriminant analysis. The decoding accuracy for the healthy individual was (84.44 $\pm$ 14.56 %), whereas for the patients, it was (77.61 $\pm$ 14.76 %). The motor regions responsible for the lower limb motions in adults (right leg, left leg, and foot) are near each other [20]. The mesial surface of both hemispheres generates ipsilateral action potentials for foot movement, which overlap at the central line and are typically so deeply rooted that they are classified on the surface [21]. As a result, with current non-invasive technology, the classification for various lower limb movements is especially difficult [22]. However, this is more difficult for the lower limbs than the upper limbs due to the proximity of motor regions that control foot and knee movement. Since the foot area in motor cortex is located around the central area, there are some issues with using EEG to study neural activity during lower limb movements. This is because of the low spatial resolution and, EEG cannot accurately measure the activity of subcortical brain regions, most of the data come from activity near the surface of the skull, within the first centimeters of brain tissue. Because of the small distance between the left and right hemispheres of the motor cortex for lower limb areas, it is difficult to discriminate between left and right leg movements [5]. Further, it is worst when it comes to intralimb movements, that is movement of the same limb, such as dorsiflexion and plantar flexion of the ankle joint. However, most previous studies have focused on recognizing contralateral movements of the upper or lower limbs, that is left, and right movements. Therefore, the purpose of the present study is to investigate whether the recognition of intralimb movement via EEG signals is possible and which pattern recognition approaches are suitable for improving classification performance. In particular, dorsi-flexion and plantarflexion of the right ankle joint movement were observed. These movements are crucial for maintaining fundamental walking positions and postures. Moreover, most recent research performed the classification of each subject and reported the average classification measure. In contrast, across-subjects movement classification has seldom been reported. Therefore, both approaches were implemented to validate the selected EEG quantities and pattern recognition schemes.

2. Related work

As described previously, most related studies have focused on distinguishing between left and right movements. Therefore, this section reviews state-of-the art method of utilizing EEG signals for decoding upper and lower limb movements. Dong Liu et al. [20], extracted the SCP to decode ankle plantar flexion by implementing continuous classification and asynchronous detection. They reported an average maximum True positive rate (TPR) was 0.86 $\pm$ 0.08 for the left leg and 0.83 $\pm$ 0.09 for the right leg. A. Dillen et al. [23], investigated the feasibility of decoding lower limb movements based on EEG signals in different frequency ranges and different decoding pipelines. Then the authors reported the decoding results of each individual with the best decoding pipeline and best frequency results and the average decoding accuracies were 0.844 $\pm$ 0.088 for able-bodied participants and 0.845 $\pm$ 0.085 for amputees. These results reveal a large diversity of decoding accuracies and best frequencies among the subjects.

R. Chaisaen et al. [24] investigated the differences in cortical activation between standing and sitting, and how the brain's intention modulates the premovement sensorimotor rhythm as they do for switching movements. This study aims to decode continuous EEG rhythms during action observation, motor imagery, and motor execution for standing and sitting. The results demonstrated that ERD was prominent during action observation, whereas ERS was typical during MI at the alpha band across the sensorimotor area. The study also used a combination of the filter bank common spatial pattern (FBCSP) and support vector machine (SVM) for classification for both offline and classifier testing analyses.

Additionally, J. H. Jeong et al. [25] presented a research study on developing a brain-machine interface (BMI) based on

movement-related cortical potentials (MRCP) to decode user intentions in real-world environments. The authors proposed a subject-dependent and section-wise spectral filtering (SSSF) method that considers the in-dividual MRCP characteristics of the subjects in different temporal sections. The proposed method was evaluated using data acquired during self-initiated walking in a powered exoskeleton environment. The results show a statistically significant improvement compared to previous methods and successful decoding results in a pseudo-online analysis.

On the other hand, G. Zhang et al. [26] presented a method for distinguishing between left- and right-hand movements using EEG signals. They used the LSTM model with an attention mechanism to learn from the temporal patterns of the EEG signals. They also extracted various features from the different bands of EEG signals in both time and frequency domains and used them to train the LSTM network for the classification task. Furthermore, they validated their approach for intra-subject and across subjects. The results showed that the intra-subject accuracy was 98.3 $\pm$ 0.9 % using the LSTM + attention mechanism. However, the accuracy dropped to 83.2 $\pm$ 1.2 % for the across-subject scheme.

Additionally, some systems that use EEG signals to classify different types of brain activity rely on decoding the signals generated when a person imagines moving different parts of their body, such as their hands, feet, or tongue [27,28]. These signals are used to infer the intended output command [29], although they may not match what the person wants to do. These signals are used because they cause different regions of the brain's outer layer, called the cerebral cortex, to become active, and these regions are far enough apart from each other that they can be easily distinguished by the EEG sensors [30,31]. However, this approach has some drawbacks, as these imagined movements are often unrelated to the actual instructions that the person wants to give to the system, and maintaining these mental images for a long time is neither natural nor comfortable for the user.

For decoding the movements of the same limb, various studies have the majority of research sought to extract various movement-related features, such as temporal and spectral features [32,33], phase-lock based features [34], and time-frequency (TF) map features of each source signal in the motor cortex [35]. Other research has proposed the use of other neural network designs for feature extraction and classification, such as the EEGNet compact convolutional neural network [36] and deep ConvNets [37]. Previous research has yielded promising results in identifying two-class hand movements with one hand, with a classification accuracy of approximately 80 %. However, the accuracy of multi-class hand motions of one hand ranged between 50 % and 70 %, which was insufficient to justify the use of rehabilitation training [38]. R. Ma et al. [39], developed an EEG-BCI paradigm that matched the steps of both one-sided lower and opposite-sided upper limb motions (also known as compound-limb movements). They evaluated the efficacy of this paradigm under two conditions: motor execution (ME) and motor imagery (MI). They employed three techniques to extract characteristics from EEG signals: common spatial pattern (CSP), subject-specific CSP (SSCSP), and filter-bank CSP (FBCSP). The SSCSP approach achieved the highest average classification accuracy of 89.02 % $\pm$ 12.84 % for ME and 73.70 % $\pm$ 12.47 % for MI in compound-limb paradigms. Motor imagery task showed lower recognition accuracy in comparison with that in the motor execution task. For instance, unilateral upper limb movement recognition paradigm was proposed by Y. Chu et al. [40], developed a feature learning approach to recognize six types of motor imagery tasks, such as elbow flexion/extension, wrist supination/protonation, and hand close/open in the unilateral upper limb. The highest accuracy of 80.50 % was achieved by SVM. Additionally, study reported by L. Gu et al. [41], compared the recognition accuracies of the motor imagery (MI) and motor execution (ME) in the lower limb movements. The mean classification accuracy across all subjects is 61.85 % for MI and 62.94 % for ME.

It be conclude from Table 1 that most of the previous studies focused on the within subjects scheme and few of these studies validated their proposed models with across subject scheme. Moreover, it is seldom to find the intralimb movement recognitions in the related work. To summarize our contributions in this work, first we utilize different EEG quantities for the intralimb movement recognition and find which quantity has the impact on the classification accuracy. Second, we validated our proposed recognition model with two data schemes: within subject and across-subject's data.

3. Methods

This section describes the data collection and preprocessing of EEG signals. Subsequently, the feature extraction and classification stages using Machine and deep learning algorithms were demonstrated. Finally, statistical comparisons were performed to explore the significance of using deep learning and an algorithm for movement recognition accuracy. The overall design of this study is depicted in

Table 1
Summary of related work.

Refer	Year	Classification scheme	Classification Performance
Dillen et al. [23]	2022	Within Subject scheme for Inter limb movement.	0.844 $\pm$ 0.088
G. Zhang et al. [26]	2019	Within Subject scheme	98.3 $\pm$ 0.9 %
		Across subjects	83.2 $\pm$ 1.2 %
Liu et al. [20]	2018	Within Subject scheme	84.44 $\pm$ 14.56 %
Tao et al. [38]	2022	Within Subject scheme	81.14 $\pm$ 6.76 %
Chaisaen et al. [24]	2020	Within Subject scheme	82.73 $\pm$ 2.54 %
J. Hoon te al [25]	2020	Within Subject scheme	86 $\pm$ 9.0 %
R. Ma [39]	2023,	Within Subject scheme	89.02 $\pm$ 12.84 %
		Unilateral Lower limb	62.68 $\pm$ 4.54 %
Yaqi Chu et al. [40]	2023	Within Subject scheme	80.50 %
L. Gu et al. [41]	2023	Within Subject scheme	62.94 %

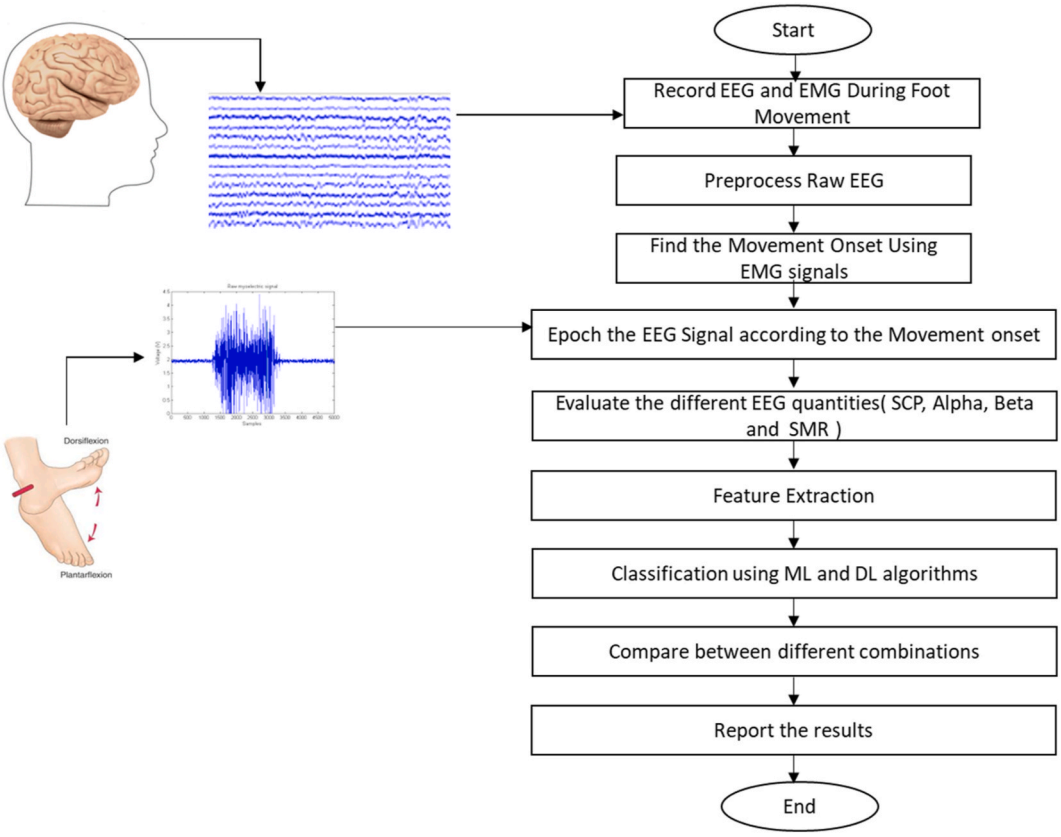

Fig. 1. General flowchart of pre-processing, feature extraction and classification.

Fig. 1.

The classification problem started by recording the EEG signal from the subject's scalp using EEG electrode during the right foot movements. EMG signals were acquired form the shank muscles to find the movement onset. Then the acquired signal passed through different preprocessing steps such as resampling, filtering, movement onset detection, artifact removal and epoching. After that, features were extracted from the processed signal and fed to the machine learning and deep learning stages.

3.1. Experimental setup and data collection protocol

Twenty-two healthy, right-handed male participants (aged 27 ± 2.9 years) participated in this study. They were chosen from undergraduate and graduate students on the campus of the Universiti PETRONAS Teknologi (UTP). For more information of the data collection procedure reader are advised to refer to our previous study [42]. The Monash University Human Research Ethics Committee approved this study (MUHREC, CF16/22165–2016001072). The experiment was conducted in accordance with the Helsinki Declarations, and all participants supplied informed written consent. Before data were collected, all participants were briefed on the procedure. This study focused on two different ankle joint motion: dorsiflexion and plantar flexion movements (DF and PF) DF represents class 1 and PF represents class 2. This arrangement allowed for a full range of motion at the ankle joints. For this movement task, the monitor was set about a meter in front of the participant. He was then instructed to move his ankle into dorsiflexion and hold the contraction for 3 s. This process was repeated until the specified number of trials (T = 25) had been completed. Following rest periods between trials, the same plantar flexion of the ankle joint was carried out. Signal Recording and Pre-processing.

Cortical and muscular signals were recorded concurrently using an NVX52 amplifier (MKS cooperation Inc., Russia).

3.1.1. EEG recording and processing procedure

The EEG data were collected from 21 channels (Fz, FC3, FC1, FCz, FC2, FC4, C5, C3, C1, Cz, C2, C4, C6, Cp5, Cp3, Cp1, Cpz, Cp2, Cp4, Cp6, and Pz) using Ag/AgCl electrodes with MCScap in line with the international 10-10 standard. The reference electrode was placed on the left and right earlobes, and the ground electrode was set between Fz and Fpz. The signal was amplified using NVX52 (MKS Cooperation Inc., Russia) and sampled at 2 kHz. Before recording the EEG signal, several steps were taken, to ensure that the electrode impedance was below 5 kΩ by injecting conductive electrogel between the EEG electrode and the scalp. The EEGlab Toolbox [34]was used in the preprocessing stage for all recorded EEG channels. First, a finite impulse response (FIR) bandpass filter was applied to the EEG signals (0.05–40 Hz). The segmented data stream was then produced (each with a duration of 4s: 1s prior and 3s after the

onset of the movement). Independent components analysis (ICA) based on the logistic infomax algorithm was utilized to eliminate discernible artifacts such as ocular motions, heart activity, and muscular contractions [34]. The ICA components containing these artifacts removed. The residual components were then projected back to induce free-form artifacts in the EEG signal. Modern BMI can distinguish between two forms of EEG rhythms that correspond to motion intention: sensorimotor rhythms (SMR) and motor related cortical potentials (MRCP). The EMG signals were recorded and processed to find the movement's onset detection. Two bipolar electrodes were placed on each muscle, Tibialis Anterior (TA) and Gastrocnemius Lateralis (GL), and the inter-electrode distance ranged from 20 to 30 mm. On the lateral malleolus, in addition to the primary sensors, a reference electrode was implanted. After being attached, the electrodes were taped together to prevent unintentional movement during the test. Then, an NVX52 amplifier (Russian Medical Computer System) was used to capture EMG signals. Throughout the data collection process, all registered signals were sampled at 2 kHz. Prior to processing the data, the EMG signals were down sampled from 2 to 1 kHz. To minimize noise levels, EMG signals were filtered using a fourth-order Butterworth bandpass filter with high and low pass cut-off frequencies of 20 Hz and 400 Hz, respectively [43]. The actual onset of the ankle movement was determined utilizing a data conditioning and threshold-based approach to the EMG signal [44].

3.1.2. EEG signal analysis

In this section, the EEG analysis process is demonstrated, and to quantify SCP, the processed EEG data were filtered at [0.1,4 Hz] with a 2nd order band pass filter. The EEG signal was segmented into 4s segments from −1 to 3 s relative to the onset of movement. Before extracting the features in the SMR including alpha (8–12) Hz, beta (13–30) Hz and both bands (8–30) Hz, the time-frequency representation of the EEG channels was analyzed to depict the EEG frequency band distributions during the movement task. Therefore, a complex Morelet wavelet convolution was employed [45]. The time-frequency representation was then produced by applying the wavelet transform to the processed EEG signals.

3.2. Feature extraction

The procedure from preprocessing to feature extraction and classification was carried out for each modality SCP, alpha, beat and SMR (Alpha beta). The features from the 21 EEG channels were evaluated over 0.25 s windows overlapped with 0.125 s. EEG features were extracted from SCP, including Permutation Entropy (PerEnt), Variance (VAR), Standard Deviation (STD), waveform length (WL) and 4th Autoregressive model (4th AR). Equations (1)–(5) list the mathematical expressions for the proposed feature. The Shannon entropy of the distribution over permutations, which can be expressed as shown in Equation (1), is the permutation entropy of the EEG signal:

$$H_n = -\sum_{\pi} p(\pi) log_2\, p(\pi) \tag{1}$$

where n is the length of the time series, π is a permutation of order D, and $p(\pi)$ is the empirical probability of π in EEG signals. The variance formula is expressed in Equation 2

$$Var = \frac{1}{n} \sum_{1}^{n} (x_i - \mu) \tag{2}$$

where n is the number of elements, x_i is the i-th element, and μ is the mean of the set whereas Equation (3) represents the waveform length

$$WL = \sum_{1}^{N} |x_i - x_{i-1}| \tag{3}$$

where N is the length of the time series, and x_i is the i-th element.

Equation (4) represents the standard formula.

$$STD = \sqrt{\frac{1}{N} \sum_{i=1}^{N} (x_i - \mu)^2} \tag{4}$$

where N is the number of samples in the signal, x_i is the value of the signal at sample i, and mu is the mean value of the signal and Equation (5) expressed the 4th order auto-regressive model.

$$x_i = -\sum_{1}^{p} a_i\, x_{i-1} + w_i \tag{5}$$

where p is the order of the model, a_i are the coefficients, x_i is the i-th element of the EEG signal, and w_i is the error term.

3.3. Classification algorithms

In this study, two different techniques, machine learning and deep learning, were utilized after feature extraction from the processed EEG signals. Two well-known machine learning classifiers, SVM and kNN, were implemented, and modified RNN deep learning models including LSTM and GRU, were employed to classify right foot movement. The results of each model are presented and compared using statistical tests.

3.3.1. Machine learning classifiers

The final stage of separating intralimb movement involves applying one of the two classification models: SVM or kNN. This study used binary class SVM classifiers with the RBF-base kernel as the basis. Equation (6) define the expression of the RBF [46]. The binary class classification accuracy on the training dataset was optimized using a smoothing parameter s with a value of 0.5.

$$k(x,y) = exp\left(\frac{-\|x-y\|^2}{2\sigma^2}\right) \tag{6}$$

where x and y represent the two data points in the feature space and σ represents the RBF's width.

The kNN method becomes more robust and reliable as a non-parametric classification algorithm when $k > 1$, as it reduces the impact of noisy points in the training set. Euclidean distance was used to measure the similarity between each trial and the training set as shown in Equation (7), and the classifier was set to output k = 3 for the highest classification accuracy [47,48].

$$d_e = \left(\sqrt{\sum_{i=1}^{N}(x_i - y_i)^2}\right) \tag{7}$$

where d_e is the Euclidean distance, x and y is two points in the feature space and N is the window length.

3.3.2. Deep learning models

Deep learning based on RNN modified models was used to classify the foot movement for intra and across-subjects' schemes. These two models were LSTM and GRU networks, respectively. A Recurrent Neural Network (RNN) is a type of neural network that can process sequential data, such as time series. However, RNNs suffer from vanishing or exploding gradients, which means that they cannot learn long-term dependencies between important events that are far apart in time.

LSTM is a special kind of RNN that solves this problem by having memory cells that can store, forget, or output values over long periods of time. LSTM network consists of LSTM blocks that have three gates: input (i_t), output (O_t), and forget gate (f_t), which control the flow of information in and out of the memory cells as depicted in Fig. 2. LSTM can preserve the error signal used to update the network weights through backpropagation through time and layers. By keeping a more stable error signal, they enable recurrent nets to learn from many time steps [49].

The cell structure consists of different parts. The cell state is output by the horizontal line at the top of the diagram, and its data can be modified or deleted by certain gates. The first interaction in the cell state is produced by the sigmoid layer, which filters out the irrelevant data from the (ht-1) and (xt) sources and discards them from the cell state (ft).

$$f_t = \sigma\left(w_f \cdot [h_{t-1}, x_t] + b_f\right) \tag{8}$$

There are two steps in the cell input selection process. A sigmoid layer determines the key values and updates the most significant ones in the first phase.

$$i_t = \sigma(w_i \cdot [h_{t-1}, x_t] + b_i) \tag{9}$$

Then in the second stage as shown in Equation (8), a tanh layer combines past information with newly created candidate data ($\widetilde{C}_t$).

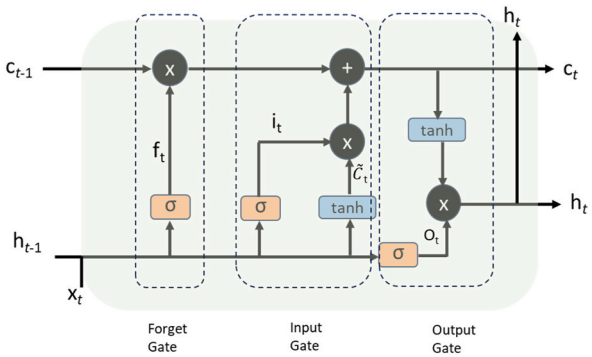

Fig. 2. Cell structure of the LSTM model.

$$\widetilde{C}_t = tanh(w_c \,.[h_{t-1}, x_t] + b_c) \tag{10}$$

As a final step, Equation (9) shows how the updated cell state Finally, the data to forget (ft) are removed and the previously selected data ($\widetilde{C}_t$). is obtained by discarding the data to forget (ft) and incorporating the previously selected data (Ct).

$$C_t = f_t * \; C_{t-1} + i_t * \; \widetilde{C}_t \tag{11}$$

A Gated Recurrent Unit (GRU) is a variant of the LSTM that is more simplified and efficient. It merges the input and forget gates into one "update gate" and adds a "reset gate" to control the information flow. The final model is less complex than standard LSTM models and is gaining more popularity [50]. A GRU, like LSTM, regulates the information inside the unit, but it does not have a separate memory cell. Fig. 3 illustrates the structure of the GRU cell.

Equation (12) through (15) illustrate how the GRU model determines the current state value ht by taking into account both new input (xt) and past information (ht-1).

$$re_t = \sigma(w_{re} \,.[h_{t-1}, x_t]) \tag{12}$$

$$u_t = \sigma(w_u \,.[h_{t-1}, x_t]) \tag{13}$$

$$\widetilde{h}_t = tanh(w_{\tilde{h}}.[re_t * h_{t-1}, x_t]) \tag{14}$$

$$h_t = (1 - \; u_t) * h_{t-1} + u_t * \widetilde{h}_t \tag{15}$$

where, w_{re} , w_u , and $w_{\tilde{h}}$ represent the weight parameters of the GRU network; re_t and u_t stand for reset and update gates, respectively. σ for sigmoid function.

For the data partitioning, 10-fold cross validation technique was applied for both schemes, within subjects and across subjects. The classification performance of the different machine learning and deep learning approaches were statistically compared by employing one paired *t*-test.

4. Results

4.1. Result of EEG signal analysis

The SCP and other EEG quantities were evaluated before the feature extraction process. Then the features were extracted from each quantity and fed to the classifiers. For instance, the average SCP was calculated in the Cz area from −1 to 3 s before the onset of the PF and DF movements is illustrated in Fig. 4. Negative deflection in both motions was first observed before the beginning of the motion and reached its minimum deflection immediately after the start of the motion. In 0.16 s following the onset of the PF movement, the SCP reached its maximum negative peak (MP) of −11.47 μV. In contrast, the maximum negative deflection during DF movements occurred at 0.2 s and −9.46 μV.

4.2. Time frequency analysis results

Fig. 5 illustrates the average TF plot over the participants of the EEG channels in the right and left motor cortex during the ankle joint motion. The phenomenon that causes a drop in power in the alpha and beta bands (8–12 Hz and 13–30 Hz, respectively) is referred to as event related desynchronization. The blue color represents this phenomenon. ERD. While the red color shows an increase in power and reflects the event-related synchronization ERS. The changes were assessed in relation to the baseline interval preceding the onset of the movement. In addition, the ERD can be seen to be at its most prominent between the frequencies of 8 and 30 Hz, as

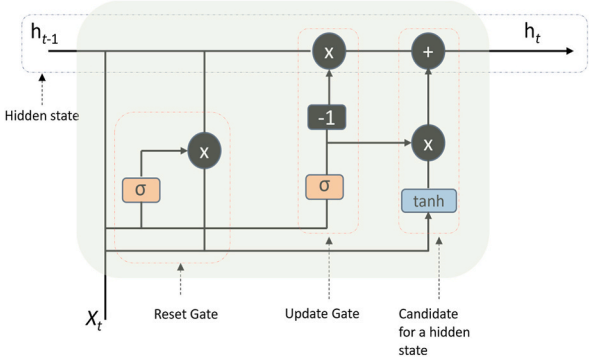

Fig. 3. Cell structure of the GRU model.

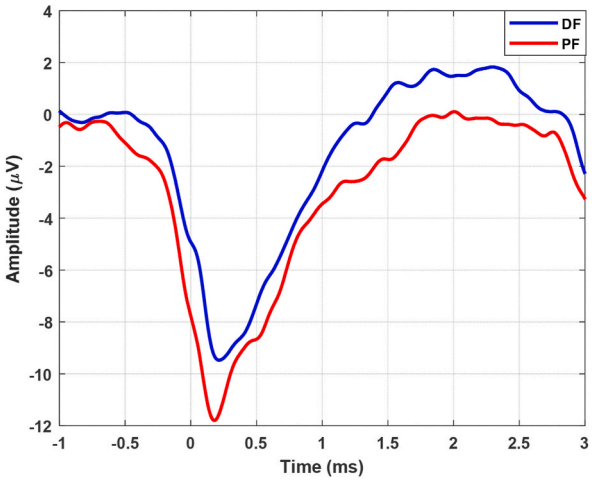

Fig. 4. The Average SCP of the PF and DF in the Cz area.

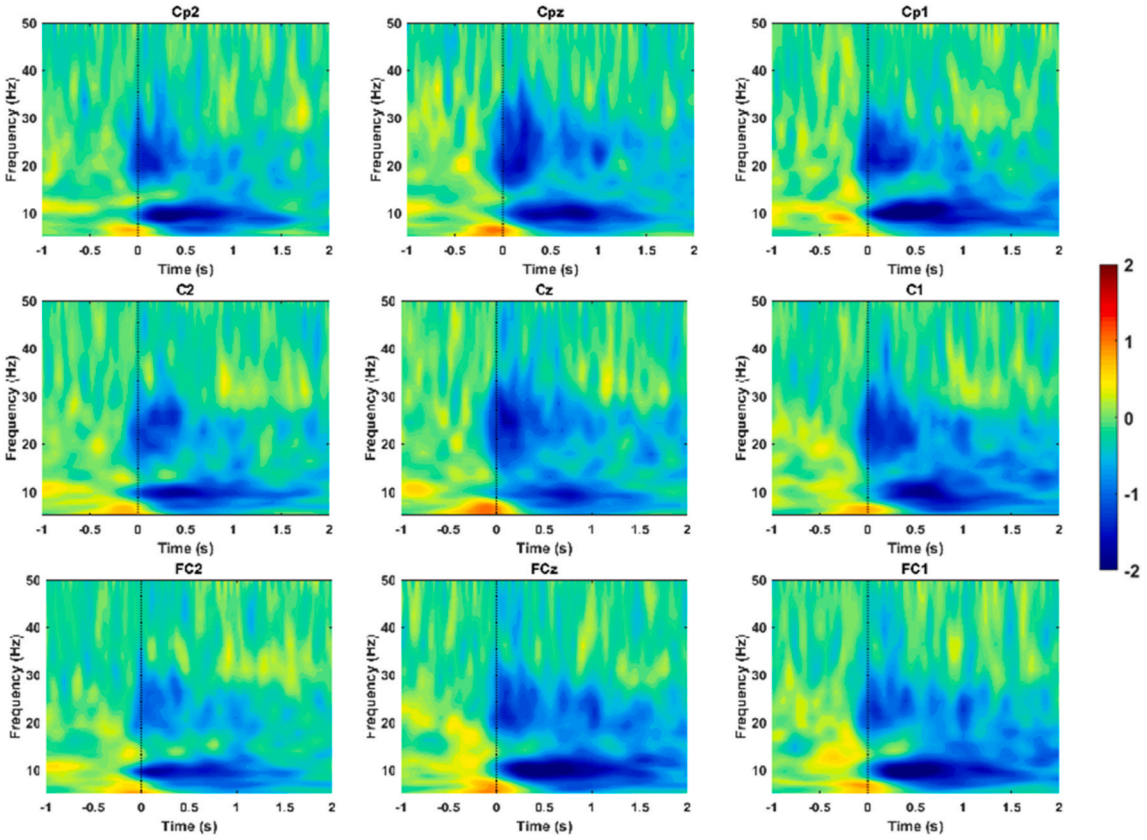

Fig. 5. The Average Time-frequency Map representation of the motor cortex area.

shown in Fig. 5.

Fig. 5 also shows that alpha and beta are the main bands that changed during the foot movements. Where the activity of the movement was associated with the desynchronization in both alpha and beta band and then synchronization started with end of the movement task.

4.3. Feature extraction and classification results

4.3.1. Within subjects classification results

Table 2 demonstrates the average classification performance of the intralimb movement of the right foot (DF and PF) using four EEG quantities: SCPs, alpha band, beta band, and SMR of both alpha and beta bands and four different classifiers including nonlinear SVM, kNN, GRU and LSTM. The SCP band reported the lowest classification performance among all EEG quantities regardless of classification algorithms. On the other hand, Beta band outperformed the other EEG quantities with both machine learning and deep learning approaches. In terms of classification algorithms, both LSTM and GRU achieved better than kNN and SVM.

Table 2 shows that there are significant differences in the accuracy, sensitivity, and specificity among different combinations of EEG bands and classifiers. For instance, the classification performance was enhanced where the accuracy increased from 82.57 % using SCP and SVM to 91.98 % when implementing GRU model with SCP. Whereas the performance of the classification was better for the alpha band in comparison to SCP where the differences is around 7.5 % when using kNN and 3.5 % for SVM. Similarly, the beta band outperformed the other bands and recorded the highest accuracy for all the classifiers models with a ($p < 0.00001$). particularly, GRU model recorded the highest classification performance in contrast with the SVM and kNN. Despite the superiority of the GRU, the differences in the classification performance with LSTM were insignificant.

Table 3 lists the p-values of the different combinations of EEG quantities and classifiers algorithms in contract with GRU model. The *p*-values reflects the significance of the classification performance enhancement using GRU model. Expect for those of the LSTM where the differences were insignificant.

Fig. 6 illustrates a comparison of the classification accuracy for the EEG bands with different classification models.

4.3.2. Across-subjects classification results

The details listed in Table 4 compared the four algorithms for EEG classification: SVM, kNN, GRU, and LSTM. Similarly, for the within-subject scheme four EEG quantities were used: SCP, Alpha, Beta, and SMR to examine the classification performance of right foot movements. In contrast to the within subject scheme results, the classification performance dropped from (10–20) % in average for the different classification models. Nevertheless, the LSTM model was superior to the other algorithms in all the classification metrics. The differences between LSTM and the other machine learning algorithms (SVM and kNN) were statistically significant as illustrated in Table 5. However, the differences between LSTM and GRU was insignificant ($p > 0.05$).

5. Discussion

This study investigated the discrimination of intralimb movement from different quantities of EEG signals and implemented different classification approaches that could improve prediction accuracy and enable the development of BCI devices for foot rehabilitation. This work aimed to recognize intralimb movement of the ankle joint using cortical signals. The acquired EEG signals were processed, and four EEG quantities were extracted, including the SCP, alpha, beta and SMR signals. These quantities were utilized to recognize intralimb movements separately. Particularly in SCPs-based classification, alpha rhythm-based classification, beta rhythm-based classification and SMR-based classification. Furthermore, the intralimb movements were used in across-subjects and within-subjects classification experiments. The features from the EEG data were extracted using four time-domain features and the fourth autoregressive model. For the goal of classification, an LSTM model and GRU were used, and two machine learning classifiers were used for comparison and to highlight the importance of utilizing a deep learning technique.

The SCP-based classification showed the lowest performance among the EEG quantities regardless of the classification model. This low recognition accuracy is because motor areas that enable movement of the lower limb are located in close proximity to each other. The slow cortical changes linked to movement preparation in the time domain are represented by SCPs [51]. For both ankle joint movements, the MP during PF movement was greater than that during DF movement. The peak of the MRCP occurred 0.16 s after movement commencement, with a maximum peak (MP) of −11.47 μV during the PF. During the DF movements, the maximum negative deflection reached −9.46 μV MP at 0.2 s. The magnitude of the negativity of the MRCPs can be correlated with the amount of

Table 2
Classification performance metrics (Average value for within-subject scheme).

EEG quantities	Classification metrics	SVM Mean ± Std	kNN Mean ± Std	GRU Mean ± Std	LSTM Mean ± Std
SCP	Accuracy (%)	82.57 ± 13.21	82.94 ± 13.96	91.98 ± 8.25	91.37 ± 9.17
	Sensitivity (%)	81.84 ± 14.88	83.85 ± 13.35	92.58 ± 7.02	91.97 ± 8.17
	Specificity (%)	83.99 ± 13.2	82.22 ± 14.64	91.70 ± 9.65	91.02 ± 10.06
Alpha	Accuracy (%)	86.89 ± 9.63	90.26 ± 8.26	97.56 ± 4.03	97.67 ± 3.06
	Sensitivity (%)	87.35 ± 9.87	91.30 ± 7.08	97.81 ± 2.75	97.70 ± 3.15
	Specificity (%)	88.72 ± 10.98	89.45 ± 9.61	97.45 ± 5.13	97.67 ± 3.19
Beta	Accuracy (%)	89.16 ± 9.18	92.711 ± 7.32	**99.18 ± 1.28**	98.87 ± 1.80
	Sensitivity (%)	88.46 ± 10.2	94.12 ± 6.43	**99.19 ± 1.31**	98.70 ± 1.80
	Specificity (%)	91.63 ± 10.73	91.45 ± 8.82	**99.24 ± 1.2**	99.02 ± 1.87
SMR	Accuracy (%)	88.14 ± 8.79	91.92 ± 7.10	98.76 ± 2.03	98.57 ± 2.18
	Sensitivity (%)	87.66 ± 8.71	92.78 ± 6.60	98.79 ± 2.09	98.52 ± 2.22
	Specificity (%)	90.64 ± 10.8	91.12 ± 8.51	98.78 ± 2.03	98.66 ± 2.15

Table 3
Statistical Comparison of Different classification algorithms' performance with GRU model.

	p - values				
		SCP	Alpha	Beta	SMR
KNN	Accuracy	2.72E-05	7.82E-06	8.73E-05	2.15E-05
	Sensitivity	3.66E-05	8.62E-06	2.68E-04	1.96E-05
	Specificity	4.03E-05	2.92E-05	1.33E-04	9.62E-05
SVM	Accuracy	1.02E-05	1.34E-07	9.92E-06	6.38E-07
	Sensitivity	7.53E-05	7.95E-06	3.54E-05	1.32E-06
	Specificity	1.04E-03	7.95E-05	1.41E-03	4.85E-04
LSTM	Accuracy	1.09E-02	**0.334**	0.041	**0.0832**
	Sensitivity	0.0181	**0.3173**	0.0237	0.0430
	Specificity	**0.05769**	**0.3427**	**0.1341**	**0.2598**

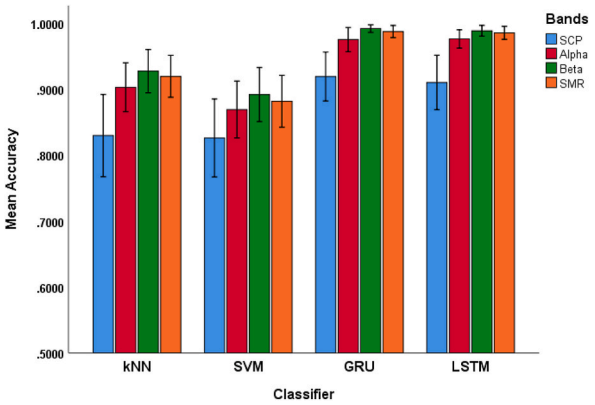

Fig. 6. Classification Comparison of different machine and deep learning models.

Table 4
Classification performance metrics (Average value for across-subjects scheme).

EEG quantities	Classification metrics	SVM	kNN	GRU	LSTM
SCP	Accuracy (%)	62.30 ± 1.79	61.60 ± 0.91	67.55 ± 3.35	70.49 ± 1.15
	Sensitivity (%)	65.55 ± 2.96	62.87 ± 2.66	74.20 ± 9.43	70.34 ± 4.48
	Specificity (%)	59.55 ± 4.67	60.45 ± 1.63	61.06 ± 14.3	71.46 ± 3.15
Alpha	Accuracy (%)	64.40 ± 1.35	67.81 ± 1.24	78.50 ± 2.31	79.95 ± 3.54
	Sensitivity (%)	66.63 ± 2.62	72.08 ± 1.63	80.53 ± 4.88	78.78 ± 8.81
	Specificity (%)	62.36 ± 2.23	63.52 ± 1.63	76.52 ± 8.6	81.39 ± 3.16
Beta	Accuracy (%)	71.34 ± 1.53	69.12 ± 1.51	86.44 ± 0.69	**87.38 ± 0.86**
	Sensitivity (%)	66.70 ± 1.27	74.96 ± 2.38	87.28 ± 1.34	**87.17 ± 0.78**
	Specificity (%)	76.04 ± 3.08	63.23 ± 2.07	85.58 ± 1.10	**87.57 ± 1.82**
SMR	Accuracy (%)	69.30 ± 1.34	68.90 ± 1.57	85.95 ± 0.90	87.08 ± 1.20
	Sensitivity (%)	64.86 ± 2.36	75.49 ± 1.97	86.04 ± 1.52	88.25 ± 1.76
	Specificity (%)	73.98 ± 2.48	61.99 ± 2.12	85.87 ± 1.63	85.90 ± 1.38

Table 5
Statistical Comparison of Different classification algorithms' performance with LSTM model.

	p-values				
		SCP	Alpha	Beta	SMR
KNN	Accuracy	9.81E-10	3.52E-06	1.98E-10	1.70E-11
	Sensitivity	4.30E-05	0.0413	5.19E-08	5.84E-10
	Specificity	8.42E-06	3.01E-10	3.01E-10	8.08E-11
SVM	Accuracy	2.26E-07	5.90E-07	1.42E-09	6.66E-11
	Sensitivity	0.0493	8.15E-08	7.41E-14	9.86E-10
	Specificity	2.71E-04	8.15E-08	5.45E-06	1.26E-07
GRU	Accuracy	0.021	**0.177**	0.025	6.89E-03
	Sensitivity	**0.104**	**0.309**	**0.398**	0.017
	Specificity	0.0282	**0.0547**	9.48E-02	**0.474**

energy required for the action, whereas the MRCPs' onset period is defined as the time spent planning and preparing the movement [52]. Numerous studies [53,54] have used MRCPs for movement intention detection and recognition. According to Ref. [53], self-paced upper limb reaching movements can be identified with approximately 80 % accuracy using MRCP pre-movement correlations. In a recent related study, the properties of MRCPs were also used to predict single-trial foot torque movement. Depending on the wavelet employed and the classification procedure, the classification accuracy is approximately 84.2 %. A recent study focusing on recognizing pre-movement states from MRCP correlations when executing ankle dorsiflexion reveals a movement execution success rate of 82.5 % [55]. In comparison with the related work, our proposed work based on the time domain features and GRU deep learning model produced higher classification performance with the SCP with an average accuracy was 87.66 %.

On the other hand, evidence from time-frequency mapping, alpha ERD, and beta ERD indicates a bilateral control phenomenon during the actual execution of movements. During movement preparation or intention, the alpha ERD was primarily contralateral, suggesting a contralateral role for brain excitability. In accordance with prior research [13], the alpha ERD observed in this investigation began in the contralateral region and became bilaterally symmetrical during movement execution. In the current work, alpha oscillations in the central brain region represented synchronized neuronal population activity. Recent research has exploited SMR in alpha and beta oscillations to detect movement intention and movement execution [56–58]. The contralateral and ipsilateral motor cortices were engaged in motor tasks, even though the SCP and SMR characteristics in lateralization phenomena differed. The coordination of motor tasks requires brain networks within and across hemispheres for both bilateral and unilateral movements [59]. Recognitions in the beta band have the highest classification accuracies than other EEG quantities, with an accuracy of 97.62 %. In contrast to the within-subject scheme, the classification performance measures dropped dramatically in the across-subjects' scheme, and this conclusion was expected due to the high variability among the subjects. However, GRU and LSTM showed robust and satisfactory performance compared with kNN and SVM. In the current study, implementing deep learning approaches based on LSTM and GRU with EEG quantities significantly impacted the classification performance. Table 6 depicted the significant improvement of the proposed work in comparison with related work. Hence, the results of this study highlighted the potential of the deep learning-based approach's for speeding up the development of a BCI for lower-limb rehabilitation in the future.

Furthermore, the developed EEG systems can influence the growth of biorobotic assistive devices that can support human movements and improve quality of life. This study has some limitations; the experiments in this work were carried out with healthy subjects. Therefore, the reliability of the proposed framework remains to be tested using data from patients with movement disabilities or neuromuscular diseases. Additionally, include female subjects to the experiment will increase the robustness and make the developed model more generalized. Another limitation is that the current work was conducted offline and moving to real world and real time application is our future direction.

6. Conclusion

Robotic devices are increasingly used in rehabilitative medicine, mainly because they can be controlled by neural signals. This study demonstrated the classification of intralimb movement. Four EEG correlates, including SCP, alpha band, beta band, and SMR of (alpha and beta) bands were analyzed. The outcomes revealed that SCPs showed the lowest accuracy compared to other EEG quantities. Furthermore, the combination of the beta band and GRU and LSTM models significantly enhanced the classification accuracy in both across- and within-subjects schemes. The highest accuracy was 99.18 $\pm$ 1.28 % when the beta band and GRU were used for the within-subject scheme. In the across-subjects scheme, the LSTM and SMR band outperformed the other combinations with accuracy of 87.38 $\pm$ 0.86 %

Ethical statement

The data used in this study received the ethical approval (ethics approval number: CF16/22165–2016001072) from Monash University Human Research Ethics Committee (MUHREC). In accordance with ethical guidelines, written consent was obtained from each participant involved in this study. This consent explicitly covered participation in the research as well as the agreement for the publication of the results derived from their data.

Data availability statement

The data used in this study are not publicly available.

Table 6
Comparison of the proposed work with the related works.

Ref	Intralimb movement	Within Subject scheme	Across Subject scheme	Within Subject scheme Accuracy	Across Subject scheme Accuracy
2018, [20]				84.44 $\pm$ 14.56 %	
2019, [26]		x	x	98.3 $\pm$ 0.9 %	83.2 $\pm$ 1.2 %
2020, [24]				82.73 $\pm$ 2.54 %	
2022, [23]	x			0.844 $\pm$ 0.088	
2023, [39]	x	x	x	89.02 $\pm$ 12.84 %	62.68 $\pm$ 4.54 %
2023 [40]				80.50 %	
Our Work	x	x	x	99.18 $\pm$ 1.28 %	87.38 $\pm$ 0.86 %

CRediT authorship contribution statement

Maged S. AL-Quraishi: Writing – review & editing, Writing – original draft, Validation, Software, Resources, Methodology, Investigation, Conceptualization. **Wooi Haw Tan:** Writing – review & editing, Resources, Project administration. **Irraivan Elamvazuthi:** Writing – review & editing, Methodology, Conceptualization. **Chee Pun Ooi:** Writing – review & editing, Validation. **Naufal M. Saad:** Writing – review & editing, Validation. **Mohammed Isam Al-Hiyali:** Writing – review & editing. **H.A. Karim:** Writing – review & editing. **Syed Saad Azhar Ali:** Writing – review & editing.

Declaration of competing interest

The authors declare that they have no known competing financial interests or personal relationships that could have appeared to influence the work reported in this paper.

Acknowledgement

The authors are grateful for Multimedia University (MMU), Universiti Teknologi PETONAS (UTP) and King Fahd University of Petroleum and Mineral (KFUPM) for supporting this work.

Appendix

Confusion Matrix of the foot movement classification.

References

[1] J. Shin, J. Kwon, C.-H. Im, A ternary hybrid EEG-NIRS brain-computer interface for the classification of brain activation patterns during mental arithmetic, motor imagery, and idle state, Front. Neuroinf. 12 (2018), https://doi.org/10.3389/fninf.2018.00005.

[2] B. Blankertz, L. Acqualagna, S. Dähne, S. Haufe, M. Schultze-Kraft, I. Sturm, M. Uščumlic, M.A. Wenzel, G. Curio, K.-R. Müller, The Berlin Brain-Computer interface: progress beyond communication and control, Front. Neurosci. 10 (2016), https://doi.org/10.3389/fnins.2016.00530.

[3] L.M. Alonso-Valerdi, R.A. Salido-Ruiz, R.A. Ramirez-Mendoza, Motor imagery based brain–computer interfaces: an emerging technology to rehabilitate motor deficits, Neuropsychologia 79 (2015) 354–363, https://doi.org/10.1016/j.neuropsychologia.2015.09.012.

[4] R. Sitaram, A. Caria, N. Birbaumer, Hemodynamic brain–computer interfaces for communication and rehabilitation, Neural Network. 22 (2009) 1320–1328, https://doi.org/10.1016/j.neunet.2009.05.009.

[5] S. Ruiz, K. Buyukturkoglu, M. Rana, N. Birbaumer, R. Sitaram, Real-time fMRI brain computer interfaces: self-regulation of single brain regions to networks, Biol. Psychol. 95 (2014) 4–20, https://doi.org/10.1016/j.biopsycho.2013.04.010.

[6] H.-L. Halme, L. Parkkonen, Comparing features for classification of MEG responses to motor imagery, PLoS One 11 (2016) e0168766, https://doi.org/10.1371/journal.pone.0168766.

[7] S.T. Foldes, D.J. Weber, J.L. Collinger, MEG-based neurofeedback for hand rehabilitation, J. NeuroEng. Rehabil. 12 (2015) 85, https://doi.org/10.1186/s12984-015-0076-7.

[8] U. Chaudhary, N. Birbaumer, A. Ramos-Murguialday, Brain–computer interfaces for communication and rehabilitation, Nat. Rev. Neurol. 12 (2016) 513–525, https://doi.org/10.1038/nrneurol.2016.113.

[9] L.F. Nicolas-Alonso, J. Gomez-Gil, Brain computer interfaces, a review, Sensors 12 (2012) 1211–1279, https://doi.org/10.3390/s120201211.

[10] N. Naseer, K.-S. Hong, fNIRS-based brain-computer interfaces: a review, Front. Hum. Neurosci. 9 (2015), https://doi.org/10.3389/fnhum.2015.00003.

[11] K.-S. Hong, M.J. Khan, M.J. Hong, Feature extraction and classification methods for hybrid fNIRS-EEG brain-computer interfaces, Front. Hum. Neurosci. 12 (2018), https://doi.org/10.3389/fnhum.2018.00246.

[12] H. Li, G. Huang, Q. Lin, J.-L. Zhao, W.-L.A. Lo, Y.-R. Mao, L. Chen, Z.-G. Zhang, D.-F. Huang, L. Li, Combining movement-related cortical potentials and event-related desynchronization to study movement preparation and execution, Front. Neurol. 9 (2018), https://doi.org/10.3389/fneur.2018.00822.

[13] K. Lee, D. Liu, L. Perroud, R. Chavarriaga, J. del R. Millán, A brain-controlled exoskeleton with cascaded event-related desynchronization classifiers, Robot. Autonom. Syst. 90 (2017) 15–23, https://doi.org/10.1016/j.robot.2016.10.005.

[14] B. Gudiño-Mendoza, G. Sanchez-Ante, J.M. Antelis, Detecting the intention to move upper limbs from electroencephalographic brain signals, Comput. Math. Methods Med. 2016 (2016) 1–11, https://doi.org/10.1155/2016/3195373.

[15] R. Ron-Angevin, F. Velasco-Álvarez, Á. Fernández-Rodríguez, A. Díaz-Estrella, M.J. Blanca-Mena, F.J. Vizcaíno-Martín, Brain-Computer Interface application: auditory serial interface to control a two-class motor-imagery-based wheelchair, J. NeuroEng. Rehabil. 14 (2017) 49, https://doi.org/10.1186/s12984-017-0261-y.

[16] Y. He, D. Eguren, J.M. Azorín, R.G. Grossman, T.P. Luu, J.L. Contreras-Vidal, Brain–machine interfaces for controlling lower-limb powered robotic systems, J. Neural. Eng. 15 (2018) 021004, https://doi.org/10.1088/1741-2552/aaa8c0.

[17] I.K. Niazi, N. Jiang, M. Jochumsen, J.F. Nielsen, K. Dremstrup, D. Farina, Detection of movement-related cortical potentials based on subject-independent training, Med. Biol. Eng. Comput. 51 (2013) 507–512, https://doi.org/10.1007/s11517-012-1018-1.

[18] A. Kline, C. Gaina Ghiroaga, D. Pittman, B. Goodyear, J. Ronsky, EEG differentiates left and right imagined Lower Limb movement, Gait Posture 84 (2021) 148–154, https://doi.org/10.1016/j.gaitpost.2020.11.014.

[19] T. Noda, N. Sugimoto, J. Furukawa, M. Sato, S.-H. Hyon, J. Morimoto, Brain-controlled exoskeleton robot for BMI rehabilitation, in: 2012 12th IEEE-RAS International Conference on Humanoid Robots (Humanoids 2012), IEEE, 2012, pp. 21–27, https://doi.org/10.1109/HUMANOIDS.2012.6651494.

[20] D. Liu, W. Chen, K. Lee, R. Chavarriaga, F. Iwane, M. Bouri, Z. Pei, J. del R. Millan, EEG-based lower-limb movement onset decoding: continuous classification and asynchronous detection, IEEE Trans. Neural Syst. Rehabil. Eng. 26 (2018) 1626–1635, https://doi.org/10.1109/TNSRE.2018.2855053.

[21] P. Bhattacharya, M. Viceconti, Multiscale modeling methods in biomechanics, WIREs Syst. Biol. Med. 9 (2017), https://doi.org/10.1002/wsbm.1375.

[22] Y. Yu, L. Fan, S. Kuang, L. Sun, F. Zhang, The research of sEMG movement pattern classification based on multiple fused wavelet function, in: 2015 IEEE International Conference on Cyber Technology in Automation, Control, and Intelligent Systems (CYBER), IEEE, 2015, pp. 487–491, https://doi.org/10.1109/CYBER.2015.7287987.

[23] A. Dillen, E. Lathouwers, A. Miladinović, U. Marusic, F. Ghaffari, O. Romain, R. Meeusen, K. De Pauw, A data-driven machine learning approach for brain-computer interfaces targeting lower limb neuroprosthetics, Front. Hum. Neurosci. 16 (2022), https://doi.org/10.3389/fnhum.2022.949224.

[24] R. Chaisaen, P. Autthasan, N. Mingchinda, P. Leelaarporn, N. Kunaseth, S. Tammajarung, P. Manoonpong, S.C. Mukhopadhyay, T. Wilaiprasitporn, Decoding EEG rhythms during action observation, motor imagery, and execution for standing and sitting, IEEE Sensor. J. 20 (2020) 13776–13786, https://doi.org/10.1109/JSEN.2020.3005968.

[25] J.-H. Jeong, N.-S. Kwak, C. Guan, S.-W. Lee, Decoding movement-related cortical potentials based on subject-dependent and section-wise spectral filtering, IEEE Trans. Neural Syst. Rehabil. Eng. 28 (2020) 687–698, https://doi.org/10.1109/TNSRE.2020.2966826.

[26] G. Zhang, V. Davoodnia, A. Sepas-Moghaddam, Y. Zhang, A. Etemad, Classification of hand movements from EEG using a deep attention-based LSTM network, IEEE Sensor. J. 20 (2020) 3113–3122, https://doi.org/10.1109/JSEN.2019.2956998.

[27] L. Cao, B. Xia, O. Maysam, J. Li, H. Xie, N. Birbaumer, A synchronous motor imagery based neural physiological paradigm for brain computer interface speller, Front. Hum. Neurosci. 11 (2017), https://doi.org/10.3389/fnhum.2017.00274.

[28] R. Zhang, Y. Li, Y. Yan, H. Zhang, S. Wu, T. Yu, Z. Gu, Control of a wheelchair in an indoor environment based on a brain–computer interface and automated navigation, IEEE Trans. Neural Syst. Rehabil. Eng. 24 (2016) 128–139, https://doi.org/10.1109/TNSRE.2015.2439298.

[29] B.J. Edelman, B. Baxter, B. He, EEG source imaging enhances the decoding of complex right-hand motor imagery tasks, IEEE Trans. Biomed. Eng. 63 (2016) 4–14, https://doi.org/10.1109/TBME.2015.2467312.

[30] E. Abdalsalam M, M.Z. Yusoff, D. Mahmoud, A.S. Malik, M.R. Bahloul, Discrimination of four class simple limb motor imagery movements for brain–computer interface, Biomed. Signal Process Control 44 (2018) 181–190, https://doi.org/10.1016/j.bspc.2018.04.010.

[31] D. Wang, D. Miao, G. Blohm, Multi-class motor imagery EEG decoding for brain-computer interfaces, Front. Neurosci. 6 (2012), https://doi.org/10.3389/fnins.2012.00151.

[32] J. Wang, L. Bi, W. Fei, C. Guan, Decoding single-hand and both-hand movement directions from noninvasive neural signals, IEEE Trans. Biomed. Eng. 68 (2021) 1932–1940, https://doi.org/10.1109/TBME.2020.3034112.

[33] R. Alazrai, H. Alwanni, M.I. Daoud, EEG-based BCI system for decoding finger movements within the same hand, Neurosci. Lett. 698 (2019) 113–120, https://doi.org/10.1016/j.neulet.2018.12.045.

[34] A. Delorme, S. Makeig, EEGLAB: an open source toolbox for analysis of single-trial EEG dynamics including independent component analysis, J. Neurosci. Methods 134 (2004) 9–21, https://doi.org/10.1016/j.jneumeth.2003.10.009.

[35] N. Mammone, C. Ieracitano, F.C. Morabito, A deep CNN approach to decode motor preparation of upper limbs from time–frequency maps of EEG signals at source level, Neural Network. 124 (2020) 357–372, https://doi.org/10.1016/j.neunet.2020.01.027.

[36] V.J. Lawhern, A.J. Solon, N.R. Waytowich, S.M. Gordon, C.P. Hung, B.J. Lance, EEGNet: a compact convolutional neural network for EEG-based brain–computer interfaces, J. Neural. Eng. 15 (2018) 056013, https://doi.org/10.1088/1741-2552/aace8c.

[37] R.T. Schirrmeister, J.T. Springenberg, L.D.J. Fiederer, M. Glasstetter, K. Eggensperger, M. Tangermann, F. Hutter, W. Burgard, T. Ball, Deep learning with convolutional neural networks for EEG decoding and visualization, Hum. Brain Mapp. 38 (2017) 5391–5420, https://doi.org/10.1002/hbm.23730.

[38] Y. Tao, W. Xu, G. Wang, Z. Yuan, M. Wang, M. Houston, Y. Zhang, B. Chen, X. Yan, G. Wang, Decoding multi-class EEG signals of hand movement using multivariate empirical mode decomposition and convolutional neural network, IEEE Trans. Neural Syst. Rehabil. Eng. 30 (2022) 2754–2763, https://doi.org/10.1109/TNSRE.2022.3208710.

[39] R. Ma, Y.-F. Chen, Y.-C. Jiang, M. Zhang, A new compound-limbs paradigm: integrating upper-limb swing improves lower-limb stepping intention decoding from EEG, IEEE Trans. Neural Syst. Rehabil. Eng. 31 (2023) 3823–3834, https://doi.org/10.1109/TNSRE.2023.3315717.

[40] Y. Chu, X. Zhao, Y. Zou, W. Xu, G. Song, J. Han, Y. Zhao, Decoding multiclass motor imagery EEG from the same upper limb by combining Riemannian geometry features and partial least squares regression, J. Neural. Eng. 17 (2020) 046029, https://doi.org/10.1088/1741-2552/aba7cd.

[41] L. Gu, J. Jiang, H. Han, J.Q. Gan, H. Wang, Recognition of unilateral lower limb movement based on EEG signals with ERP-PCA analysis, Neurosci. Lett. 800 (2023) 137133, https://doi.org/10.1016/j.neulet.2023.137133.

[42] M.S. Al-Quraishi, I. Elamvazuthi, T.B. Tang, M. Al-Qurishi, S. Parasuraman, A. Borboni, Multimodal fusion approach based on EEG and EMG signals for lower limb movement recognition, IEEE Sensor. J. 21 (2021) 27640–27650, https://doi.org/10.1109/JSEN.2021.3119074.

[43] S.A. Go, K. Coleman-Wood, K.R. Kaufman, Frequency analysis of lower extremity electromyography signals for the quantitative diagnosis of dystonia, J. Electromyogr. Kinesiol. 24 (2014) 31–36, https://doi.org/10.1016/j.jelekin.2013.11.002.

[44] S. Solnik, P. Rider, K. Steinweg, P. DeVita, T. Hortobágyi, Teager–Kaiser energy operator signal conditioning improves EMG onset detection, Eur. J. Appl. Physiol. 110 (2010) 489–498, https://doi.org/10.1007/s00421-010-1521-8.
[45] E. Formaggio, S. Masiero, A. Bosco, F. Izzi, F. Piccione, A. Del Felice, Quantitative EEG evaluation during robot-assisted foot movement, IEEE Trans. Neural Syst. Rehabil. Eng. 25 (2017) 1633–1640, https://doi.org/10.1109/TNSRE.2016.2627058.
[46] C.-C. Chang, C.-J. Lin, Libsvm, ACM Trans. Intell. Syst. Technol. 2 (2011) 1–27, https://doi.org/10.1145/1961189.1961199.
[47] N.K. Al-Qazzaz, Z.A.A. Alyasseri, K.H. Abdulkareem, N.S. Ali, M.N. Al-Mhiqani, C. Guger, EEG feature fusion for motor imagery: a new robust framework towards stroke patients rehabilitation, Comput. Biol. Med. 137 (2021) 104799, https://doi.org/10.1016/j.compbiomed.2021.104799.
[48] R. Rana, Gated Recurrent Unit (GRU) for Emotion Classification from Noisy Speech, 2016.
[49] Y. Yu, X. Si, C. Hu, J. Zhang, A review of recurrent neural networks: LSTM cells and network architectures, Neural Comput. 31 (2019) 1235–1270, https://doi.org/10.1162/neco_a_01199.
[50] S. Gao, J. Yang, T. Shen, W. Jiang, A parallel feature fusion network combining GRU and CNN for motor imagery EEG decoding, Brain Sci. 12 (2022) 1233, https://doi.org/10.3390/brainsci12091233.
[51] J.G. Colebatch, Bereitschaftspotential and movement-related potentials: origin, significance, and application in disorders of human movement, Mov. Disord. 22 (2007) 601–610, https://doi.org/10.1002/mds.21323.
[52] D.J. Wright, P.S. Holmes, D. Smith, Using the movement-related cortical potential to study motor skill learning, J. Mot. Behav. 43 (2011) 193–201, https://doi.org/10.1080/00222895.2011.557751.
[53] M.S. Mirzaee, S. Moghimi, Detection of reaching intention using EEG signals and nonlinear dynamic system identification, Comput. Methods Progr. Biomed. 175 (2019) 151–161, https://doi.org/10.1016/j.cmpb.2019.04.023.
[54] M. Jochumsen, C. Rovsing, H. Rovsing, I.K. Niazi, K. Dremstrup, E.N. Kamavuako, Classification of hand grasp kinetics and types using movement-related cortical potentials and EEG rhythms, Comput. Intell. Neurosci. 2017 (2017) 1–8, https://doi.org/10.1155/2017/7470864.
[55] S. Aliakbaryhosseinabadi, N. Jiang, A. Vuckovic, K. Dremstrup, D. Farina, N. Mrachacz-Kersting, Detection of movement intention from single-trial movement-related cortical potentials using random and non-random paradigms, Brain-Comp. Interf. 2 (2015) 29–39, https://doi.org/10.1080/2326263X.2015.1053301.
[56] S.Yu Gordleeva, M.V. Lukoyanov, S.A. Mineev, M.A. Khoruzhko, V.I. Mironov, A.Ya Kaplan, V.B. Kazantsev, Exoskeleton control system based on motor-imaginary brain–computer interface, Sovremennye Tehnologii v Med. 9 (2017) 31, https://doi.org/10.17691/stm2017.9.3.04.
[57] M.S. Al-Quraishi, I. Elamvazuthi, T.B. Tang, M. Al-Qurishi, S. Parasuraman, A. Borboni, Detection of lower limb movements using sensorimotor rhythms, in: 2020 8th International Conference on Intelligent and Advanced Systems (ICIAS), IEEE, 2021, pp. 1–5, https://doi.org/10.1109/ICIAS49414.2021.9642696.
[58] D.P. Murphy, O. Bai, A.S. Gorgey, J. Fox, W.T. Lovegreen, B.W. Burkhardt, R. Atri, J.S. Marquez, Q. Li, D.-Y. Fei, Electroencephalogram-based brain–computer interface and lower-limb prosthesis control: a case study, Front. Neurol. 8 (2017), https://doi.org/10.3389/fneur.2017.00696.
[59] Q. Lin, H. Li, Y.-R. Mao, W.-L. Lo, J.-L. Zhao, L. Chen, Y. Leng, D.-F. Huang, L. Li, The difference of neural networks between bimanual antiphase and in-phase upper limb movements: a preliminary functional, Magnet. Resonan. Imag. Study Behav. Neurol. 2017 (2017) 1–9, https://doi.org/10.1155/2017/8041962.